van der Waals states in ozone and their influence on the threshold spectrum of $O_3(X^1A_1)$. I. Bound states

Sergy Yu. Grebenshchikov,[a] Reinhard Schinke, and Paul Fleurat-Lessard
Max-Planck-Institut für Strömungsforschung, D-37073 Göttingen, Germany

Marc Joyeux
Laboratoire de Spectrométrie Physique (CNRS UMR 5588), Université Joseph Fourier-Grenoble I, BP 87, 38402 St. Martin d'Heres Cedex, France

(Received 17 June 2003; accepted 3 July 2003)

Threshold spectra of several isotopomers of ozone are studied using accurate quantum mechanical calculations and an *ab initio* potential energy surface. Shallow van der Waals minima in the dissociation channels, separated from the deep main wells by an 80 cm^{-1} high barrier, are shown to accommodate long progressions of assignable states. As a result, dense vibrational spectrum of ozone near dissociation is dominated by van der Waals-type states for all studied isotope compositions. © *2003 American Institute of Physics.* [DOI: 10.1063/1.1603737]

I. INTRODUCTION

Studies of highly vibrationally excited molecular eigenstates near dissociation threshold is one of the central topics in modern chemical dynamics (see, for example, Refs. 1–3, and references therein). The reason is that chemical and physical properties of highly energized molecules differ dramatically from their features near the equilibrium. For example, the familiar normal mode assignment of vibrational spectra often becomes inappropriate at threshold. Furthermore, new types of vibrational states appear at high energies. They can come into existence as a result of ''bifurcations'' in the existing progressions triggered by sudden changes in the classical phase space.[3] Such bifurcations were documented and analyzed for many triatomic molecules including HCP,[2] HOCl,[4] H_3^+,[5] and HOBr.[6] Alternatively, new molecular states can emerge in those regions of the intramolecular potential, which become accessible only at threshold. Loosely bound orbiting states in nitrogen dioxide, held together by long range electrostatic forces, is a good case in point.[7,8] van der Waals states in ozone, the main subject of the present article, furnish another example.

Our interest in threshold spectra of isotopically substituted ozone is stimulated by recent attempts to explain the anomalous isotope effect in this molecule. The effect, observed in the formation of ozone upon $O+O_2$ collisions in the Earth's atmosphere,[9] is presently under extensive experimental[10–12] and theoretical[13] investigation. At room temperature, the collision energy of reactants is small ($k_BT \approx 200\ cm^{-1}$) and the reaction dynamics is sensitive to the properties of low-lying metastable rovibrational states (resonances). In particular, the energy window immediately adjacent to threshold seems to be of prime importance: Experimental studies[11] revealed a direct correlation between the relative formation rate coefficients and the tiny ($\sim 22\ cm^{-1}$) differences between the zero point energies of the reactants and products in exchange reactions.

One of the explanations of the observed isotope effect is put forward by Gao and Marcus[13] and is based on the statistical RRKM theory. It successfully accounts for the measured formation rates, yet requires an adjustable ''nonstatistical'' correction factor intended to parametrize dynamical differences between different isotopomers. At the moment it is not clear to which extent the RRKM model is applicable to the largely nonstatistical ozone molecule.[14] However, this theory indicates the key ''coarse grained'' quantities which can control the formation rate at threshold: the density of rovibrational states and the average lifetime of the activated complex. The dependence of the threshold densities and lifetimes on the isotope constitution deserves a detailed quantum mechanical investigation which goes beyond statistical models.

States of ozone near the dissociation threshold remain little investigated. There are no high resolution spectroscopic measurements in this energy range. In regard to theory, two quantum mechanical studies have been performed recently using an accurate *ab initio* potential energy surface (PES).[14,15] While Siebert *et al.* gave a detailed analysis of the spectrum of $^{16}O^{16}O^{16}O$ in a broad energy range and showed that many vibrational bound states and metastable resonances in the dissociation continuum are clearly assignable,[14] they did not specifically consider the energies around dissociation threshold. This was done in another study, in which Babikov *et al.*[15] employed a slightly modified version of original PES from Ref. 14 and calculated resonance states in the first 60 cm^{-1} above threshold. They found that the resonance spectra of $^{16}O^{16}O^{18}O$ and $^{16}O^{18}O^{18}O$ isotopomers are qualitatively different from the spectrum of $^{16}O^{16}O^{16}O$; the former two were significantly more dense than the latter and consisted of a series of states with large lifetimes, especially in the narrow energy window of 22 cm^{-1} above threshold. This energy window corresponds exactly to the difference in zero point energies of oxygen diatoms in the hetero- and homonuclear dissociation channels. This remarkable finding

[a]Author to whom correspondence should be addressed. Electronic mail: sgreben@gwdg.de

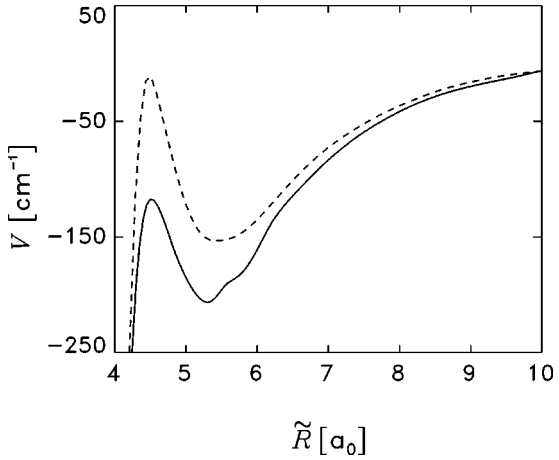

FIG. 1. A cut through the ozone potential along the minimum energy path to dissociation (solid line). The distance between the O atom and the center of mass of the O_2 diatom is taken as the dissociation coordinate $\tilde{R}$. Dashed line shows the lowest adiabatic potential curve in the entrance channel $^{16}O + {}^{16}O^{18}O$. The potential along the MEP is shifted vertically so that the asymptotic values of the two curves coincide. $E=0$ corresponds to the lowest quantum mechanical threshold.

might serve as a basis for a fully quantum mechanical description of the isotope effect.[16,17] However, several essential questions have not been addressed in Ref. 15. First and foremost, the nature of the additional states at threshold still remains unclear, as well as the physical reasons for the high threshold density of states in isotopically substituted ozone. Answers to these questions are of considerable importance in defining the role of the extra threshold states in ozone formation: They allow one to evaluate the probability, with which these states can be populated in an $O+O_2$ collision.

This paper is the first in a series of two describing ozone states at dissociation threshold. Our main result, which follows from the detailed analysis of the PES and the eigenfunctions, is that the accumulation of vibrational states at threshold is intimately related to another—extremely interesting and hitherto not discussed—feature of ozone, namely, the existence of loosely bound van der Waals (vdW) states in a narrow energy strip of about 150 cm^{-1} around threshold. This feature is shared by ozone molecules in *all* isotopic combinations, including $^{16}O^{16}O^{16}O$. We first deal with the bound part of the vdW spectrum. Metastable resonances immediately above threshold are analyzed in the subsequent publication.[18]

The key factor leading to the appearance of vdW states is the shape of the PES in the asymptotic region. In Fig. 1, the potential energy profile is shown along the minimum energy path (MEP) in one of the entrance channels. At about 5.5 bohr, the asymptotic potential has a shallow minimum mainly caused by long range quadrupole–quadrupole and dispersion interactions between O and O_2.[19] The minimum lies approximately 210 cm^{-1} below the asymptote, and yet its depth is significantly smaller: It is controlled by the barrier separating the vdW minimum from the main ozone well, which is only 80 cm^{-1} high. Another factor contributing to the trapping of vibrational states in the vdW minimum is the coupling between the dissociation coordinate and the hindered O_2 rotation. This coupling creates a high *dynamical* barrier preventing particles in vdW minima from entering the main wells. One way to show this is to adiabatically separate the rotation of O_2 in the vibrational ground state from the motion along the dissociation coordinate,[20] as is commonly done in SACM theory.[21] The lowest adiabatic potential curve (Fig. 1), acting as an effective potential near threshold, has a pronounced barrier of nearly 140 cm^{-1}. Full quantum calculations, performed for total angular momentum $J=0$, confirm that vibrational vdW states are nested in the minimum and, to a large extent, remain independent of the states in main wells. As will be shown below, vdW states dominate the spectrum of nonrotating ozone at threshold, regardless of the isotope composition. In particular, they increase the threshold density of states by almost a factor of 10.

Bound and resonance states in shallow vdW minima have been previously investigated for other molecular systems. The best studied, both theoretically and experimentally, are vdW complexes.[22–24] The main distinction between the physically bound complexes and O_3 is that in ozone the vdW states are found at the same energies at which bound eigenstates of chemically bound ozone exist. The role of weak vdW interactions has also been extensively discussed in the context of reactive scattering at low energies. For example, near-threshold long lived resonance states were recently calculated in the vdW minima in the entrance and exit channels of the reaction $O+HCl\rightarrow OH+Cl$.[25] These states were shown to produce sharp structures in the cumulative reaction probability, at least for $J=0$. Resonances above vdW minima were also seen in the benchmark reaction $F+H_2$.[26] Finally, vdW forces were at the heart of explanation of the observed dynamical isotope effect in the reaction between Cl and HD.[27] The role of vdW states in the oxygen exchange reactions and the formation of O_3 remains to be investigated. In fact, the present study is the first in which these states are reported and characterized. It is worth mentioning, however, that the possibility of formation of weakly bound ozone complexes was mentioned in Ref. 28 in connection with the observed anomalous pressure dependence of the falloff curves.

Five isotopomers of ozone have been studied at threshold in the course of preparation of this paper: $^{16}O^{16}O^{16}O$, $^{16}O^{16}O^{18}O$, $^{16}O^{18}O^{16}O$, $^{16}O^{18}O^{18}O$, and $^{18}O^{16}O^{18}O$. Two of them consisting of two ^{16}O atoms and one atom ^{18}O, i.e., $^{16}O^{16}O^{18}O$ and $^{16}O^{18}O^{16}O$, are selected to be the main illustrative examples throughout the paper. Properties of other isotope combinations, also summarized below, are similar.

The paper is organized as follows: First, details of the quantum calculations on the global PES are given in Sec. II. Vibrational vdW progressions calculated in one isolated asymptotic channel are then briefly sketched in Sec. III in order to pave the way for a detailed analysis of the threshold spectra on the global PES presented in Sec. IV. In conclusion, the influence that overall rotation and nonadiabatic interactions might have on vdW dynamics are discussed in Sec. V.

II. DETAILS OF DYNAMICS CALCULATIONS

Eigenstates of the molecular Hamiltonian for the total angular momentum $J=0$ have been calculated in the energy

range of 200 cm^{-1} around the quantum mechanical threshold. In these calculations, the PES of Ref. 14 was employed with the modifications as described in Ref. 15. This is the most accurate ozone potential to date, which reproduces the measured eigenenergies within 4–5 cm^{-1} (see Ref. 14) up to about 85% of the experimental dissociation energy. The PES is constructed from the *ab initio* data[14] calculated at the MRCI level with the Davidson correction (MRCI+Q) using the quadruple zeta cc-pVQZ basis set of Dunning.[29] In the vicinity of the transition state barrier and in the asymptotic vdW region, the potential is further adjusted[15] to include the results of even higher level calculations and extrapolation to the complete basis set limit.[20] Topological features of the PES relevant for this study are specifically addressed in Sec. IV A.

The Schrödinger equation was solved using filter diagonalization (FD).[30,31] This method is well suited for calculating vibrational states at threshold, where the density of states is high and the convergence is therefore difficult to achieve with direct diagonalization. FD is performed in two steps. First, a (narrow) energy window $[E_{\min}, E_{\max}]$ is preselected and a basis set $\{\Psi_i\}$, optimal for this window, is generated by applying the filtering operator $\mathrm{Im}\,\hat{G}^+(E_i)=\mathrm{Im}(E_i-\hat{H}_0-\mathrm{i}W)^{-1}$ onto an initial wave packet χ ($E_{\min}\leqslant E_i\leqslant E_{\max}$). The complex absorbing potential $\mathrm{i}W$ is set to zero for calculations of bound states. The filtering is performed by expanding the Green's function $\hat{G}^+(E_i)$ in terms of (modified) Chebyshev polynomials.[32] In the next step, the Hamiltonian matrix in the basis $\{\Psi_i\}$ is diagonalized giving the eigenenergies and the corresponding wave functions. The number of basis functions depends on the number of eigenstates in a given energy window and is usually quite small, of the order of 10^2. In our calculations, the threshold region was split into four overlapping windows ranging in size from 120 cm^{-1} at lower energies to 40 cm^{-1} at threshold. Between 120 and 190 basis functions were used in each window. The number of Chebyshev terms necessary to produce a convergent representation of the Green's function was about 200 000.

Most calculations were performed in Jacobi coordinates as described in Ref. 14. For a molecule in equilibrium, R is defined as the distance between the central oxygen atom and the center of mass of the two side atoms; r corresponds to the distance between the two side atoms, and γ is the angle between **R** and **r**. Ozone has three distinct equilibrium geometries, differing in permutations of the oxygen atoms. For a combination of two ^{16}O atoms and one ^{18}O, two equilibria correspond to $^{16}O^{16}O^{18}O$, while the third one describes the symmetric molecule $^{16}O^{18}O^{16}O$. At energies far below threshold, transitions between different permutations are energetically forbidden and the dynamics in each well are uncorrelated. At threshold, different wells are connected through the asymptotic vdW minima in the dissociation channels and, strictly speaking, isomerization between different permutations can take place (see Ref. 33 and the discussion in Sec. IV A below). It is therefore necessary to consider all permutations within a single quantum calculation. The Jacobi coordinates described above cover the whole configuration space and are suitable for our purposes. However, the domain of variation of the two stretching coordinates has to be unusually large to include three main ozone wells as well as three vdW regions in the asymptotic channels.

The kinetic and potential energy operators were expressed in the discrete variable representation.[34] In the largest calculations, the following grid parameters were adopted: $0.1\,a_0\leqslant R\leqslant 21.0\,a_0$ with 290 potential optimized points[35] and $1.3\,a_0\leqslant r\leqslant 23.0\,a_0$ with 300 potential optimized points. Only those points were retained in the grid, whose potential energy was below $V_{\mathrm{cut}}=1.7$ eV ($E=0$ corresponds to an infinite distance between O and O_2 with O_2 at equilibrium). These grid extensions in R and r ensure that the vibrational states in all vdW minima are converged to at least 10^{-2} cm^{-1}. Indeed, as will be shown below, some of these states lie only 1 cm^{-1} below threshold. This implies that the bound-state wave functions can penetrate into the classically forbidden region over the distances of more than $10\,a_0$.

Proper choice of the coordinate system enables one to halve the angular grid and thus noticeably reduce the computational effort. For the $^{16}O_2{}^{18}O$ isotopomer, it is convenient to place the ^{18}O atom in the apex and take R as a vector connecting ^{18}O with the center of mass of $^{16}O_2$. The well located around $\gamma=\pi/2$ will be that of $^{16}O^{18}O^{16}O$ and is C_{2v} symmetric. The other two wells, both describing asymmetric ozone with ^{18}O as a side atom and located at $\gamma\approx\pi/6$ and $\gamma\approx 5\pi/6$, are related to each other through a symmetry transformation $\gamma\rightarrow\pi-\gamma$ which is equivalent to the permutation of the side atoms. As a result, the full Hamiltonian splits into two blocks, the one which is symmetric with respect to $\gamma\rightarrow\pi-\gamma$ (overall parity $P=+1$), and another, antisymmetric block ($P=-1$). For all isotope combinations considered, this symmetry can be incorporated in the numerical grid in much the same way as it was recently done for H_2O (Ref. 36; see also Ref. 37 for a general discussion of the symmetry adapted DVR). The angular coordinate is represented by 75 Gauss–Legendre quadrature points[38] in the interval $0\leqslant\gamma\leqslant\pi/2$ and the kinetic energy matrices in angle are correspondingly symmetrized to include Legendre polynomials of either even (for $P=+1$) or odd order (for $P=-1$). Calculations for different parities are performed separately.

Additionally, we investigated the spectra of vdW wells in a single dissociation channel. These ''restricted'' calculations help to estimate the expected threshold density of vdW states and to classify the states in vibrational progressions. The restricted calculations were performed in Jacobi coordinates $(\tilde{R},\tilde{r},\tilde{\gamma})$ appropriate for the dissociation channel under consideration. For the $^{16}O^{18}O+{}^{16}O$ channel, $\tilde{R}$ is the distance between ^{16}O and the center of mass of $^{16}O^{18}O$, $\tilde{r}$ is the bond length of the diatom and $\tilde{\gamma}$ is the angle between the two vectors. The dissociation coordinate $\tilde{R}$ was allowed to vary between $4.4\,a_0$ and $23\,a_0$, with 270 potential optimized points. For the other two coordinates the grid parameters were as follows: $1.9\,a_0\leqslant\tilde{r}\leqslant 3.0\,a_0$ with 16 potential optimized points and $0\leqslant\tilde{\gamma}\leqslant\pi$ with 100 Gauss–Legendre points. Only 70 000 Chebyshev iterations were necessary to obtain a fully converged spectrum.

The set of Jacobi coordinates $(\tilde{R},\tilde{r},\tilde{\gamma})$ was also used in

the global calculations to check the convergence of the eigenstates with respect to grid parameters. These convergence tests, performed up to energies of $50\ \mathrm{cm}^{-1}$ below threshold, are based on the notion that the converged spectrum must be independent of the coordinate system chosen to represent the Hamilton operator. In $\tilde{R}$, 140 potential optimized DVR points were taken in the interval $(0.1\ a_0, 10\ a_0)$, $\tilde{r}$ was represented on an optimized grid of 140 points in the interval $(1.3\ a_0, 12\ a_0)$, while $\tilde{\gamma}$ ranged from 0 to π and included 130 Gauss–Legendre points. Again, the resulting eigenstates belong to either $P=+1$ or $P=-1$ symmetry blocks, although the DVR basis was not symmetry adapted in these test calculations. The eigenstates were assigned by visual inspection of the three-dimensional wave functions and compared with their counterparts calculated in another coordinate system. For all energy windows, the uncertainty introduced by changing the Jacobi set never exceeded $0.05\ \mathrm{cm}^{-1}$. Closer to threshold (i.e., for energies above $-50\ \mathrm{cm}^{-1}$) such tests became too time consuming.

III. VAN DER WAALS STATES IN ONE DISSOCIATION CHANNEL

The asymptotic $O\cdots O_2$ potential in one arrangement channel is sketched in the upper left frame of Fig. 2 in Jacobi coordinates $(\tilde{R},\tilde{\gamma})$; the bond length $\tilde{r}$ of the diatom is fixed at the equilibrium distance of $2.28\ a_0$. The potential is plotted only for $\tilde{R}\geqslant 4.4\ a_0$, and the main ozone wells are not shown. The two minima, symmetric about $\tilde{\gamma}=90°$, correspond to the two equivalent bent vdW equilibria; they lie $210\ \mathrm{cm}^{-1}$ below the asymptote. The asymptotic part of the surface has several saddle points. The highest are the barriers at linearity, $\tilde{\gamma}=0°$ and 180° ($150\ \mathrm{cm}^{-1}$ with respect to the vdW minimum). The saddle at $\tilde{\gamma}=90°$, separating the equilibrium vdW geometries, describes a T-shaped transition state and lies $120\ \mathrm{cm}^{-1}$ above minima. The two symmetric saddle points at $\tilde{R}\approx 4.5\ a_0$ connecting vdW wells with the main ozone minima are the lowest: their height is only $80\ \mathrm{cm}^{-1}$.

These shallow wells support relatively long vibrational progressions. For all isotope combinations but one, we found 22 bound vdW states between the minimum and the quantum mechanical threshold; for $^{16}O\cdots{}^{16}O^{16}O$ the number of bound vdW states is 21. Most of the states (18 out of 22 for $^{16}O\cdots{}^{16}O^{18}O$, for example) belong to pure progressions of either $\tilde{R}$ or $\tilde{\gamma}$. Typical wave functions are illustrated in Fig. 2. The properties of the spectrum, e.g., the transition frequencies, the assignments, and the energetic order of states, depend only weakly on the isotope composition. Common to all vdW states is their ''two-dimensional'' character: Excitations occur solely in $\tilde{R}$ and $\tilde{\gamma}$, while the almost completely decoupled high frequency O_2 oscillator is in the ground vibrational state and plays no role in the dynamics. The two fundamental frequencies are very low, $\omega_{\tilde{R}}\sim 40\ \mathrm{cm}^{-1}$ and $\omega_{\tilde{\gamma}}\sim 60\ \mathrm{cm}^{-1}$, slightly depending on the oxygen masses. Moreover, the modes are strongly anharmonic, especially in $\tilde{R}$: Already the third pure excitation has a frequency of only

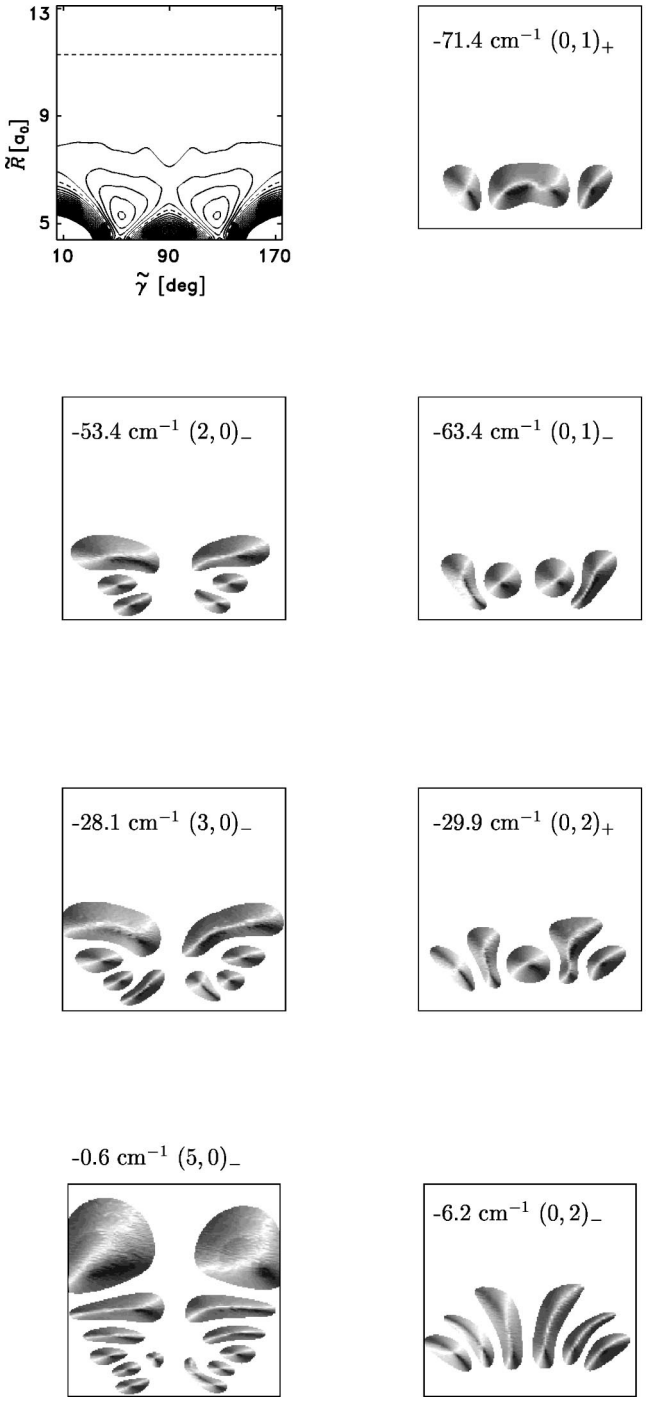

FIG. 2. Examples of wave functions in two vibrational progressions in the vdW well in the arrangement channel $^{16}O\cdots{}^{16}O^{18}O$ calculated on a spatially restricted grid as described in Sec. II. Shown in Jacobi coordinates $(\tilde{R},\tilde{r},\tilde{\gamma})$ is one particular contour $\epsilon(\tilde{R},\tilde{r},\tilde{\gamma})=|\Psi(\tilde{R},\tilde{r},\tilde{\gamma})|^2=\mathrm{const}$, with the constant value being the same in all frames. The $\tilde{\gamma}$ axis ranges from 5° to 175° and the $\tilde{R}$ axis ranges from $4.4\ a_0$ to $13.1\ a_0$. The plots are viewed along $\tilde{r}$, in the direction perpendicular to the plane of the other two axes. Shading emphasizes the 3D character of the plots. The eigenenergy in each frame is measured with respect to the quantum mechanical threshold for the channel. Vibrational assignments are given in parentheses. The potential in $(\tilde{R},\tilde{\gamma})$ coordinates with $\tilde{r}$ fixed at $2.28\ a_0$ is shown in the upper left frame. The contour spacing is 5 meV and the lowest energy is -25 meV. The dashed line denotes the contour $E=0$. Potential energy is normalized in such a way that $E=0$ corresponds to O_2+O with O_2 at equilibrium.

$25\ \mathrm{cm}^{-1}$. This explains the rather large number of states in the vdW minima.

From the third state up, the vdW spectrum lies above the saddle point on the path leading to the main ozone well. Remember that an infinite wall is placed at $\tilde{R}=4.4\ a_0$ in these calculations, and the wave functions cannot reach the inner part of the potential. In order to check whether they are really localized in the asymptotic region, we first repeated the calculations with the infinite wall slightly shifted inward to $\tilde{R}=4.2\ a_0$. The energies of bound states changed by less than $0.5\ \mathrm{cm}^{-1}$. Compared to the transition frequencies, this variation is small, which indicates that even above the saddle point the eigenstates in vdW minima are effectively uncoupled from the inner wells. Unrestricted calculations on the global PES (Sec. IV) confirm this conclusion. In the adiabatic approximation, coupling between $\tilde{R}$ and $\tilde{\gamma}$ creates a dynamic barrier between the inner and the outer parts of the potential. The height of this effective hindered rotation barrier, estimated from the adiabatic curve in Fig. 1, is $140\ \mathrm{cm}^{-1}$, nearly twice as large as that of the bare potential. It is this barrier, behind which the vdW states are trapped.

All bound states in the vdW spectra can be assigned vibrational quantum numbers $(n_{\tilde{R}},n_{\tilde{\gamma}})$ (the third quantum number, $n_{\tilde{r}}$, equals zero). The wave functions, together with their assignments, are exemplified in Fig. 2. Since the complex $^{16}O\cdots{}^{16}O^{18}O$ is not symmetric, the amplitudes of eigenstates in the left-hand and the right-hand wells are not exactly the same. However, at energies near and above the saddle separating the two wells, the symmetry is almost restored and eigenstates have either a node or a maximum near $\tilde{\gamma}=90°$. We denote the former states with an additional index "$-$" (antisymmetric), while the latter states have index "$+$" (symmetric). For truly symmetric complexes, for example $^{16}O\cdots{}^{18}O^{18}O$, this notation becomes exact. The assignment of states shown in Fig. 2 is rather straightforward: One counts the number of nodes along the nodal line in one well. Intramode coupling forces the nodes of pure stretching wave functions (Fig. 2, left column) to substantially deviate from a straight line. The effect of coupling becomes even more pronounced for combination states, not shown in Fig. 2. Their assignment is no longer trivial and should be based on the structure of the underlying periodic orbits in the vdW wells. The relation between the classical and quantum dynamics in the vdW wells, along with the residual isotope-dependent effects in the vdW spectra, will be analyzed in the forthcoming publication.[39] The pure bending mode (Fig. 2, right column) remains almost unaffected by coupling with $\tilde{R}$ even near threshold. One expects to find such localized states—in the form of narrow resonances—also above threshold.

The low fundamental frequencies and the large anharmonicities in vdW minima lead to a high density of states. Figure 3 shows, for $^{16}O\cdots{}^{16}O^{18}O$, that the vibrational states tend to accumulate in the vicinity of the quantum mechanical threshold. Similar patterns are observed for all other isotopes. At threshold, the density of vdW states in one arrangement channel reaches $0.5\ \mathrm{per\ cm}^{-1}$. Extrapolation into the dissociation continuum predicts even higher values in the first $20\ \mathrm{cm}^{-1}$ above D_0.

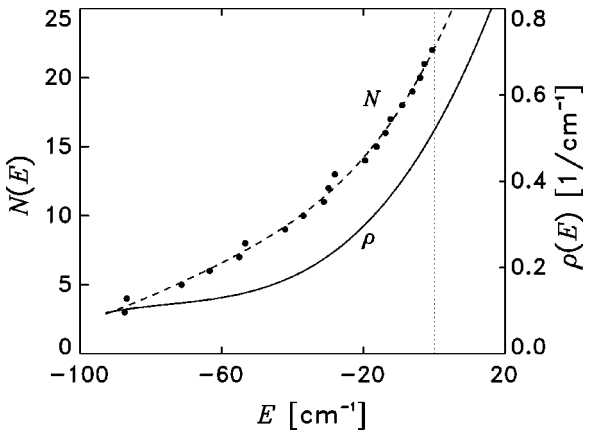

FIG. 3. Quantum mechanical number of vdW states, $N(E)$, in the arrangement channel $^{16}O\cdots{}^{16}O^{18}O$ below threshold (dots) and the fit according to the equation $N(E)=\Sigma_{i=1}^{4}a_i E^i$ (dashed line). The density of quantum states $\rho(E)=dN/dE$ is shown with a solid line. The vertical dotted line marks the position of the quantum mechanical threshold.

IV. VAN DER WAALS STATES ON THE GLOBAL PES

The threshold spectrum of ozone is more complicated than the pure vdW spectrum described in the previous section. The true spectrum comprises the states localized in the main ozone well and the vdW states in the two dissociation channels attached to this well. Mixings between the two types of eigenstates and the possibility of ozone isomerization further increase the complexity of the spectrum. We start the discussion of threshold eigenstates by a short description of the topography of the global PES (Sec. IV A). The quantum results are then presented in Sec. IV B.

A. Topography of the global PES

The coordinate grid in the quantum calculations covers the whole configuration space of the molecule, including all three possible conformations and the three dissociation channels. Figure 4 illustrates how the various potential wells and arrangement channels in $^{16}O^{16}O^{18}O$ are connected. Shown in Fig. 4(a) is a polar plot of the PES in hyperspherical coordinates $(\rho,\ \chi)$, as defined in Ref. 40. The second angle θ is fixed at the C_{2v} equilibrium value for O_3. The three main minima (traced by thick contour lines) correspond to the three stable ozone isomers, one with ^{18}O in the apex, and the other two with ^{18}O as a side atom (these two are, of course, identical). Far below threshold, each potential well supports an independent spectrum, characteristic of the ozone molecule in question and observable by means of high resolution spectroscopy.[41] Near threshold, the main wells are linked through the shallow vdW double wells (thick contour lines between the main wells). In other words, the three different oxygen permutations are connected through common asymptotic channels.

Two hyperspherical coordinates are insufficient for a simultaneous description of both the inner part of the potential and the asymptotic region: The third coordinate, θ, should also be allowed to vary. For the purposes of further discus-

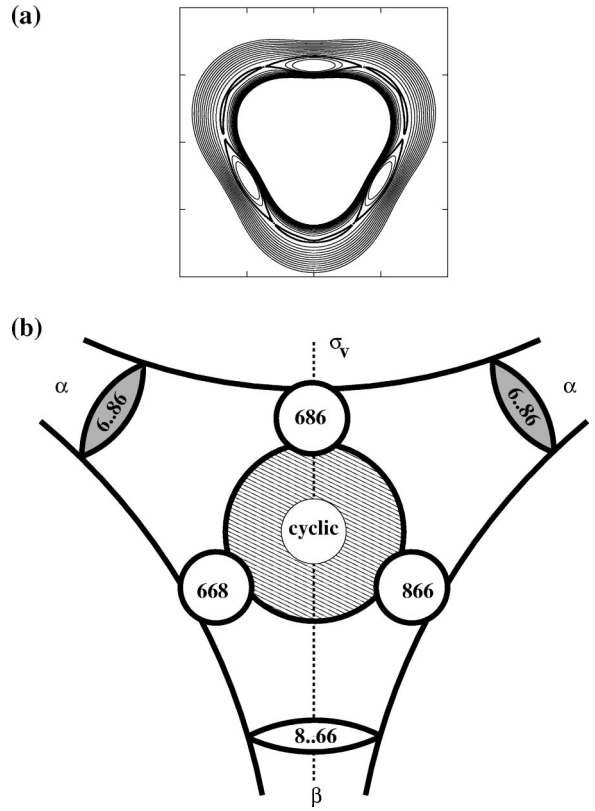

FIG. 4. Topography of the ozone potential. (a) Polar plot of the PES in hyperspherical coordinates (ρ,χ). The angle θ is fixed at 40°. The maximum hyperradius ρ is 7.0 a_0. The lowest contour level is -0.2 eV, and the contours are separated by 0.2 eV. The thick line marks the three equivalent ozone minima and the connecting vdW wells. The central minimum, corresponding to cyclic ozone, is not shown. (b) Schematic representation of various constituents of the PES for the isotope combination ^{16}O, ^{16}O, and ^{18}O. The three stable isomers (main minima) are shown with circles and labeled 686, 866, and 668. The middle hatched area indicates a high barrier separating the main minima and encircling the cyclic structure. Heteronuclear (α) and homonuclear (β) dissociation channels are separated from the main minima by vdW regions labeled 6..86 and 8..66. Shading indicates that the quantum thresholds and the vdW vibrational ground states in channels α have lower energy than in the channel β. The vertical dashed line denotes the symmetry axis.

sion one needs only consider a two dimensional schematic representation as shown in Fig. 4(b). Its inner part, modeling the hyperspherical plot, is augmented by three asymptotic channels, separated from the main wells by regions containing shallow vdW minima. One dissociation channel and the corresponding vdW region are shared by two adjacent main wells. The metastable cyclic ozone trapped behind a high potential barrier in the center of the plot is not considered in this paper. The symmetry properties of the diagram in Fig. 4(b) coincide with those of the Hamiltonian in the Jacobi set (R,r,γ) used in the global calculations. The main symmetry element is the plane σ_v crossing the plane of the plot at a right angle along the dashed line. All eigenstates can be classified as either symmetric $(P=+1)$ or antisymmetric $(P=-1)$ with respect to reflection in σ_v.

States localized in the main well situated on the middle line belong to the isomer ^{16}O^{18}O^{16}O denoted in Fig. 4(b) as 686. For this isomer, vibrational states with different parities correspond to either even or odd excitations of the antisymmetric stretch and are nondegenerate.[42] The eigenstates of the isomer ^{16}O^{16}O^{18}O in our calculations are delocalized over the two identical wells labeled 668 and 866. Transitions between these two wells due to under-barrier tunneling are negligible, so that the eigenstates with $P=+1$ and $P=-1$ are degenerate. Each symmetry block (for example, $P=+1$) contains the full information on the spectrum of ^{16}O^{16}O^{18}O. Since the isomer is nonsymmetric, the wave function amplitudes *in one well* possess no symmetry.

The same considerations hold for the vdW spectrum. The eigenstates $P=\pm 1$ of the complex ^{16}O$\cdots^{16}$O^{18}O are delocalized over the vdW regions in the two heteronuclear channels α. Eigenstates of different parities are degenerate in the absence of transitions between the channels. One symmetry block is sufficient to describe the whole excitation spectrum of either of the two vdW complexes. For the complex ^{18}O$\cdots^{16}$O^{16}O in the homonuclear channel β, the eigenstates are nondegenerate. Symmetry block $P=+1$ contains states with an even number of bending quanta, while $P=-1$ contains odd bending excitations (cf. assignments in Sec. III).

The diagram in Fig. 4(b) shows how the main minima are connected through vdW regions. For example, the 668 well is linked to its mirror image 866 through the vdW complex 8..66 in the homonuclear channel β, while the two spectroscopically different species, 686 and 668, are linked through the complex 6..86 in the heteronuclear channel α. Mixings between the vibrational states in the main wells and the vdW states imply transitions between the ozone permutations. We shall see in the next section that at threshold, the degeneracy of the $P=\pm 1$ parity blocks in 668 and 886 wells is lifted for some states, thus leading to isomerization.

B. Spectrum of eigenstates

The vibrational states of the isotope combination of two oxygen atoms ^{16}O and one ^{18}O in the last 150 cm^{-1} below dissociation threshold are summarized in Table I. The wave functions of ''normal'' ozone are labeled according to the main well in which they are localized [see Fig. 4(b)]. Accurate vibrational assignment, still possible for some of these states, is not pursued in this study. As was already discussed in Sec. IV A, the eigenstates of ^{16}O^{16}O^{18}O are delocalized between the two symmetric wells 668 and 866. In the calculations, these states appear as doublets with parity $P=+1$ and -1. Degenerate doublets are shown in Table I as a single state with parity $P=\pm 1$. If, however, the doublets are split, each component is shown separately (these states are highlighted in boldface).

Our main finding is that vdW states can be unambiguously detected in the calculations on the global PES. These states are also presented in Table I. The notation for them includes the description of the dissociation channel in which the state is located (Greek letter) and the assignment in terms of two quantum numbers, the dissociation mode $\tilde{R}$, and the bending mode $\tilde{\gamma}$, as described in Sec. III. For example, $\alpha(0,0)$ denotes a vibrational ground vdW state in the heteronuclear channels 6..86 [cf. Fig. 4(b)]. Note that vdW states in channels α also appear in pairs, degenerate if unperturbed.

TABLE I. Vibrational eigenstates of $^{16}O^{16}O^{18}O$ and $^{16}O^{18}O^{16}O$ near dissociation threshold.

E, eV[a]	$E-D_0$, cm^{-1}	Parity	Assignment[b]	Mixing[c]	E, eV[a]	$E-D_0$, cm^{-1}	Parity	Assignment[b]	Mixing[c]
0.07615	−148.67[d]	−1	686	⋯	0.08875	−47.01	±1	866/668	⋯
0.07647	−146.09	±1	866/668	⋯	0.08934	−42.27	±1	$\alpha(1,1)_+$	⋯
0.07756	−137.29	−1	686	⋯	0.08957	−40.43	−1	$\beta(0,1)_-$	⋯
0.07853	−129.45	±1	$\alpha(0,0)$[e]	⋯	0.08977	−38.81	+1	686	⋯
0.07860	−128.89	±1	$\alpha(0,0)$[f]	⋯	**0.08993**	**−37.54**	**−1**	$\boldsymbol{\alpha(1,1)_-}$	⋯
0.07893	−126.24	+1	686	⋯	**0.09000**	**−36.94**	**+1**	$\boldsymbol{\alpha(1,1)_-}$	**686**
0.07945	−122.05	−1	686	⋯	0.09018	−35.48	+1	$\beta(2,0)_+$	866/668
0.07970	−120.04	±1	866/668	⋯	**0.09039**	**−33.76**	**−1**	**866/668**	$\boldsymbol{\beta(2,0)_-}$
0.08028	−115.37	+1	686	⋯	**0.09058**	**−32.28**	**+1**	**866/668**	⋯
0.08131	−107.02	+1	$\beta(0,0)_+$	⋯	**0.09062**	**−31.92**	**−1**	$\boldsymbol{\alpha(3,0)_+}$	**866/668; $\beta(2,0)_-$**
0.08134	−106.78	−1	$\beta(0,0)_-$	⋯	**0.09065**	**−31.68**	**+1**	$\boldsymbol{\alpha(3,0)_+}$	**866/668; 686**
0.08177	−103.28	+1	686	⋯	0.09066	−31.58	−1	$\beta(2,0)_-$	866/668
0.08204	−101.15	±1	866/668	⋯	0.09088	−29.86	±1	$\alpha(0,2)_+$	⋯
0.08269	−95.88	±1	866/668	⋯	0.09108	−28.26	±1	$\alpha(3,0)_-$	⋯
0.08270	−95.81	+1	686	⋯	0.09206	−20.31	+1	$\beta(1,1)_+$	⋯
0.08270	−95.79	−1	686	⋯	0.09208	−20.14	±1	$\alpha(2,1)_+$	866/668
0.08369	−87.84	±1	$\alpha(1,0)_+$	⋯	0.09237	−17.80	±1	$\alpha(4,0)_-C$[g]	866/668
0.08378	−87.13	±1	$\alpha(1,0)_-$	⋯	0.09261	−15.90	−1	$\beta(1,1)_-$	866/668
0.08401	−85.23	±1	866/668	⋯	0.09266	−15.50	±1	866/668	⋯
0.08441	−81.99	±1	866/668	⋯	0.09279	−14.42	±1	$\alpha(4,0)_+$	866/668
0.08537	−74.26	±1	866/668	⋯	0.09301	−12.63	±1	$\alpha(4,0)_-$	⋯
0.08573	−71.35	±1	$\alpha(0,1)_+$	⋯	0.09309	−12.01	+1	686	⋯
0.08584	−70.48	−1	686	⋯	0.09323	−10.86	+1	$\beta(3,0)_+$	⋯
0.08621	−67.55	+1	686	⋯	0.09341	−9.42	±1	$\alpha(1,2)_+$	866/668
0.08632	−66.60	+1	$\beta(1,0)_+$	⋯	0.09376	−6.65	−1	$\beta(3,0)_-$	⋯
0.08640	−65.96	−1	$\beta(1,0)_-$	⋯	0.09378	−6.46	+1	$\beta(0,2)_+$	⋯
0.08670	−63.54	±1	$\alpha(0,1)_-$	686	0.09382	−6.14	±1	$\alpha(0,2)_-$	866/668
0.08708	−60.53	−1	686	⋯	0.09388	−5.67	±1	866/668	α
0.08738	−58.10	±1	866/668	⋯	0.09410	−3.85	±1	$\alpha(3,1)_+$	866/668
0.08768	**−55.68**	**+1**	$\boldsymbol{\alpha(2,0)_+}$	⋯	**0.09424**	**−2.74**	**−1**	$\boldsymbol{\alpha(5,0)_+}$	**866/668; 686**
0.08770	**−55.47**	**−1**	$\boldsymbol{\alpha(2,0)_+}$	**686**	**0.09426**	**−2.58**	**+1**	$\boldsymbol{\alpha(5,0)_+}$	**866/668**
0.08790	**−53.89**	**+1**	$\boldsymbol{\alpha(2,0)_-}$	⋯	0.09444	−1.12	±1	$\alpha(6,0)_+$	686
0.08792	**−53.70**	**−1**	$\boldsymbol{\alpha(2,0)_-}$	**686**	0.09458	0.03	±1	$\alpha(5,0)_-$	866/66
0.08855	−48.66	+1	$\beta(0,1)_+$	⋯					

[a]Energy normalization is such that $E=0$ corresponds to an infinite separation between O and O_2 with the diatom at equilibrium.
[b]No vibrational assignments are given for the states localized in the main ozone wells. Instead, labels of the wells are shown, according to the diagram in Fig. 4(b). vdW states are assigned in terms of two quantum numbers as described in Sec. III. Additionally, the channel to which vdW state belongs is indicated with a Greek letter [see Fig. 4(b)]. For mixed states, the assignment is based on the main component of the wave function.
[c]For states delocalized between the main and the vdW wells, this entry indicates the weak component(s) of the wave function.
[d]Energy with respect to the quantum mechanical dissociation threshold D_0 (D_0 is the energy of a nonrotating O_2 diatom in the vibrational ground state). The lowest threshold for the isotope combination ^{16}O, ^{16}O, ^{18}O is $D_0=0.09458$ eV.
[e]This vdW state in the heteronuclear channel α is localized in one minimum of the double well vdW potential.
[f]This vdW state in the heteronuclear channel α is localized in the second minimum of the double well vdW potential.
[g]This vdW state is born in a bifurcation near threshold. Detailed analysis will be given elsewhere (Ref. 39).

Only those states for which the degeneracy is lifted are shown as separate entries in Table I.

The first two vdW states in the global spectrum appear 130 cm^{-1} below threshold. They belong to the heteronuclear channel 6..86 and represent ground vibrational states in either one or the other minimum of the double well vdW potential. At slightly higher energy, one finds the first two vdW states in the homonuclear channel 8..66. Up to about -65 cm^{-1} most of the states belong to the main wells. Closer to threshold, the situation is reversed: vdW states (in all channels) outnumber ''normal'' ozone states. In the last 10 cm^{-1} below D_0, the spectrum is almost entirely of the vdW type.

The data in Table I also demonstrate that the two components of the overall spectrum, vdW and ''normal,'' are largely independent: the mixing between the two classes of states is weak, especially below -40 cm^{-1}. Note that only the ground vdW states in both channels are positioned below the potential barrier to the main well. All other states lie above this barrier and can, in principle, be fully delocalized. They are kept in the vdW region by the coupling between R and γ, which leads to a high effective dynamical barrier at the transition state (see Fig. 1). As in the restricted calculations, pure bending excitations remain localized in the vdW regions up to threshold and even above it.[18] Their nodal structure is identical to the bending progression shown in Fig. 2.

Examples of vdW states, $|\Phi|^2$, in the stretching progression on the global PES are given in Fig. 5 for $^{16}O^{18}O^{16}O$ and $^{16}O^{16}O^{18}O$. The states in the left column belong to the homonuclear channel 8..66 and are the easiest to display. Due to

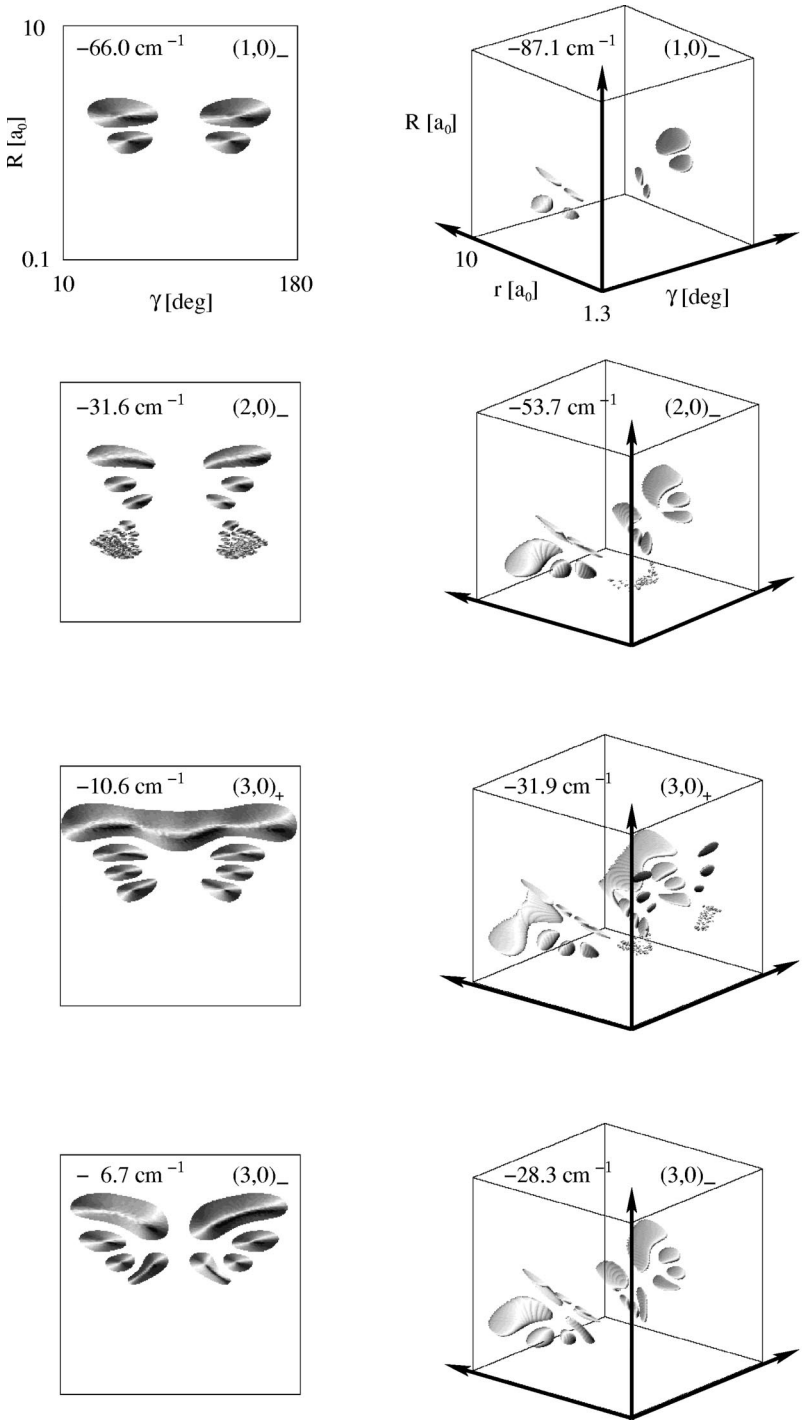

FIG. 5. Wave functions of vdW states (stretching progression) in ozone. Jacobi coordinates (R,r,γ) are used. The ranges of variation of the coordinates are the same for all wave functions; they are indicated in the upper left (for R and γ) and upper right (for r) frames. As in Fig. 2, one contour of the three-dimensional wave function is shown. The left column shows vdW states in the homonuclear channel 8..66. These plots are viewed along r, in the direction perpendicular to the plane of the other two axes. In the right column, the states in the heteronuclear channels 6..86 are depicted in the full three-dimensional representation. See text for more details. Eigenenergy in each frame is measured with respect to the lowest quantum mechanical threshold D_0. Vibrational assignments are given in parentheses.

the chosen set of Jacobi coordinates, they have the same ''two-dimensional'' appearance as the vdW states in the restricted calculations shown in Fig. 2. Three of the four shown states are of purely vdW nature. Note that the vdW states remain pure even 6.7 cm^{-1} below the lowest dissociation threshold. The state $(2,0)_-$ is mixed: it has minor components (with dense nodal structures) in two wells corresponding to the 866 and 668 molecules [cf. Fig. 4(b)]. This is probably due to an accidental resonance between the states in two parts of the configuration space.

The right column of Fig. 5 illustrates vdW states in the heteronuclear channels 6..86. We selected those states, for which the vibrational assignments are the same as for the states in the left column. In the Jacobi coordinates (R,r,γ) the states in 6..86 channels can be displayed only as fully three-dimensional objects: Dissociation channels α correspond to $R\to\infty$ and $r\to\infty$ with γ approaching either 0 or π. $|\Phi|^2$ is clearly symmetric with respect to $\gamma=\pi/2$. The directions of nodal lines indicate the directions of the stretching normal modes in each channel. The states $(1,0)_-$ and $(3,0)_-$ are decoupled from the main wells, while $(2,0)_-$ has a weak contribution of the isotopomer 686 (at $\gamma\approx\pi/2$). The state which, according to its strongest component, is assigned to $(3,0)_+$ $(P=-1)$ has the most complicated nodal structure. It is mixed with the states in the 866 and 668 wells and also contains a clearly visible trace of the vdW state $\beta(2,0)_-$

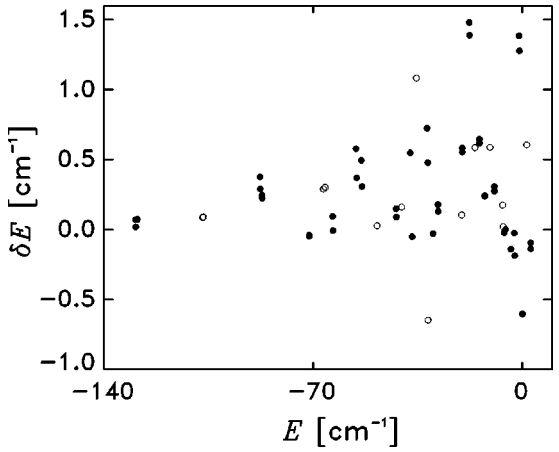

FIG. 6. The difference, δE, between the vdW eigenenergies in the global and the restricted calculations. Solid and empty circles denote the vdW states in channels 6..86 and 8..66, respectively. States of both parities, $P=\pm 1$, are shown.

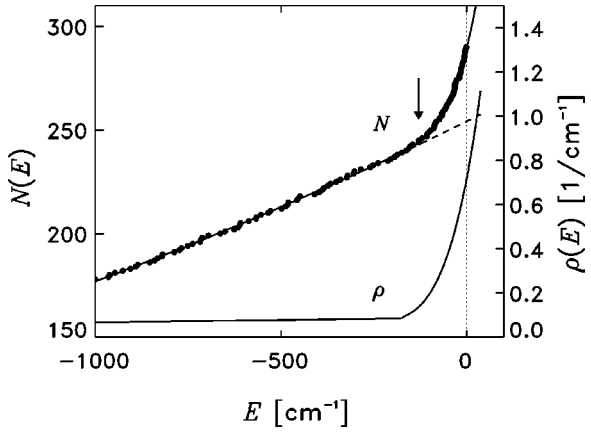

FIG. 7. Quantum mechanical number of states, $N(E)$, of $^{16}O^{16}O^{18}O$ below threshold (dots) and the fit according to the equation $N(E)=\Sigma_{i=1}^{6}a_iE^i$ (solid line). The dashed line represents a fit of $N(E)$ only up to the energy of $-200\ \mathrm{cm}^{-1}$ and its extrapolation to higher energies. The density of states $\rho(E)=dN/dE$ is shown with a solid line. The vertical dotted line marks the position of the quantum mechanical threshold. Arrow indicates the energy at which the first vdW state appears.

from the channel 8..66. ''Multicomponent'' states will be described in more detail at the end of this section.

Even in the presence of mixing, the vdW spectrum preserves its clear identity. This is evidenced by Fig. 6 in which the energies of vdW states in the global and the restricted calculations are compared. For most of the states, the difference does not exceed $0.5\ \mathrm{cm}^{-1}$; the agreement between two calculations is especially good for the states in the homonuclear channel 8..66. Larger deviations indicate more mixing with the main wells, but even then the difference remains to be bounded by only $1.5\ \mathrm{cm}^{-1}$, still less than the average distance between states in one dissociation threshold ($1/\rho \approx 2\ \mathrm{cm}^{-1}$; cf. Fig. 3). For this reason, the energetic order and the assignments of the vdW states in one particular channel in the global calculations are identical to those in the restricted calculations: the global spectrum behaves very much like a sum of spectra of isolated main wells and three independent dissociation channels. A similar statement is true of other isotopomers. In $^{16}O^{16}O^{16}O$, mixings are more pronounced and, consequently, the deviations of the restricted calculations from the global ones are larger. In $^{18}O^{16}O^{18}O$ and $^{16}O^{18}O^{18}O$ the mixings are weaker and the agreement between the restricted and global calculations is better than in Fig. 6. The localization and the very existence of distinct vdW states depend on the presence of a small barrier between the vdW region and the main ozone well. The height of this barrier was determined with an accuracy of 5 meV ($40\ \mathrm{cm}^{-1}$) in a set of extensive *ab initio* calculations.[20] However, the localization is to a large extent dynamical and, being caused by the *adiabatic* barrier, is only partly sensitive to the bare barrier height.

It is obvious from the above discussion, that vdW states dramatically modify the vibrational spectrum of ozone. The energy dependence of the number and the density of states for the isotopomer $^{16}O^{16}O^{18}O$ is presented in Fig. 7 in the interval of $1000\ \mathrm{cm}^{-1}$ below threshold. According to the diagram in Fig. 4(b), the spectrum of this molecule near threshold consists of contributions coming from the main well 668 and two vdW regions in the adjacent channels α and β. Since these contributions are almost independent of one another, one can easily select states, belonging to this isotopomer, out of the global spectrum. Shown in Fig. 7 are the $P=+1$ states of the wells 668/866, $P=+1$ vdW states belonging to the dissociation channel 6..86, and the vdW states of both parities, $P=\pm 1$, localized in the channel 8..66. Far below threshold,[43] the number of states grows almost linearly, leading to a constant density of states of about $0.08\ 1/\mathrm{cm}^{-1}$. Extrapolation to higher energies predicts the total number of states to be around 250. The vdW minima near threshold add about 40 extra states to the expected number. As a result, the density sharply rises by nearly one order of magnitude reaching the value of $0.7\ 1/\mathrm{cm}^{-1}$ at D_0.

vdW states dominate the threshold spectra of all ozone isotopomers. This is illustrated in Fig. 8, in which the spectra of the main wells and of the distinguishable vdW regions for the three different isotope combinations are summarized. The states are sorted according to the assignment of the strongest component of the underlying wave function. In each frame, the energy is normalized to the *lowest* dissociation threshold for a given isotope set. For asymmetric molecules [like 668/866 or vdW regions in channels α in Fig. 4(b)], states of only one parity block are shown. For all species in Figs. 8(a)–8(c), including the fully symmetric $^{16}O^{16}O^{16}O$, the main well supports a sparse vibrational spectrum, while the dense threshold component comes from the vdW states in the dissociation channels. In $^{16}O^{16}O^{16}O$, three wells and three vdW regions are equivalent, and it is sufficient to show only one main and one vdW spectrum [Fig. 8(a)]. A different situation arises with molecules depicted in Figs. 8(b) and 8(c). For them, the vdW spectra in the homo- and the heteronuclear channels are shifted with respect to each other. This shift amounts to about $22\ \mathrm{cm}^{-1}$ and unambiguously correlates with ΔZPE, i.e., the difference between zero-point energies of O_2 fragment diatoms in these channels; ΔZPE is at the same time the difference in positions of dissociation thresholds. For example, the quantum mechanical threshold in the

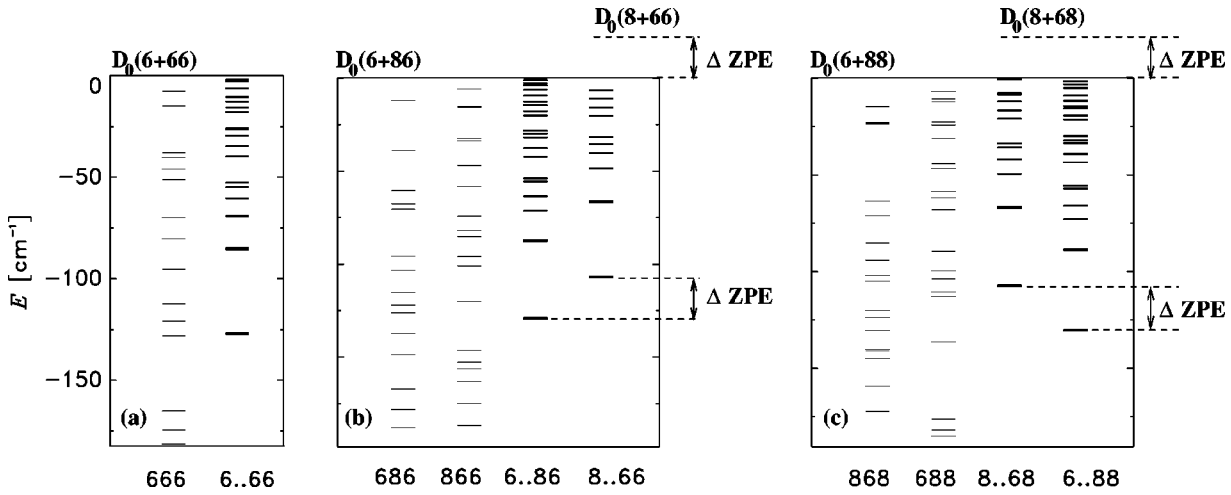

FIG. 8. Vibrational spectra near dissociation thresholds for three groups of isotopomers: (a) $^{16}O^{16}O^{16}O$; (b) $^{16}O^{18}O^{16}O$ and $^{16}O^{16}O^{18}O$; (c) $^{18}O^{16}O^{18}O$ and $^{16}O^{18}O^{18}O$. Energy zero in each frame corresponds to the lowest dissociation threshold in the group. In (b) and (c), the thresholds for the higher lying arrangement channels and the differences between the zero point energies of fragments (Δ ZPE) are also shown. Threshold energies used in this work are: $D_0(6+66)=D_0(8+66)=0.09722$ eV; $D_0(6+86)=D_0(8+68)=0.09458$ eV; $D_0(6+88)=0.09175$ eV.

channel 6..86 is 22 cm^{-1} lower than in the channel 8..66 [see Fig. 8(b); this difference is also stressed by shading in Fig. 4(b)]. Accordingly, the first vdW state in the channel 6..86 appears 22 cm^{-1} below the first vdW state in the channel 8..66. This relative shift by exactly ΔZPE is due to the fact that the O_2 stretching mode in the asymptotic channels is almost completely decoupled from the remaining two degrees of freedom.[20]

One can surmise that the sequence of vdW states will not abruptly stop at D_0. In particular, those states, that are trapped in the channel still closed [8..66 in Fig. 8(b)] will remain essentially bound. For them, dissociation becomes possible only ΔZPE above the lowest threshold—this is the energy at which ''their'' channel opens. This observation is at the heart of the physical origin of the dense resonance spectrum observed in Ref. 15 and will be discussed in detail elsewhere.[18]

In conclusion, we briefly consider the mixing patterns arising between the vdW and the ''normal'' ozone states. The simplest to analyze are the wells 866/668 and the dissociation channels α: the presence of mixing is unambiguously indicated by the splitting of the states with $P=\pm 1$.

According to the diagram in Fig. 4(b), splitting of the $P=\pm 1$ states in 866/668 result from the coupling to the homonuclear channel β. Examples are the two states at -33.76 cm^{-1} and -32.28 cm^{-1}. About 2 cm^{-1} above them, at -31.58 cm^{-1}, a vdW state $\beta(2,0)_-$ is located (parity $P=-1$). Note that only one component of the 866/668 doublet, the one with $P=-1$, can couple to this vdW state. As a result, this symmetry selective coupling leads to the splitting $\Delta\approx 1.5$ cm^{-1} in the doublet. Mixings imply isomerization between different ozone isotopomers. In the split doublets, the corresponding lifetime of a wave packet localized in one of the wells is of the order of $2\pi/\Delta\sim 22$ ps.

The splitting mechanism for the vdW states in channels α is similarly based on symmetry selection. Proper illustrations are provided by states $\alpha(1,1)_-$ and $\alpha(3,0)_+$ in Table I. The interaction between the symmetric channels is mediated by states of the 686 molecule [cf. Fig. 4(b)]. A state 686 ($P=+1$) in the vicinity of $\alpha(1,1)_-$ is in a near resonance with the $P=+1$ component of the vdW doublet thus leading to an effective shift in its energy and a doublet splitting. Even more complicated mixing patterns are observed in the calculated wave functions. They simultaneously involve several perturbing states in different main wells and/or channels [cf. the state $\alpha(3,0)_+$ in Fig. 5]. However, they can be considered as weak perturbations which leave the eigenenergies nearly unaffected. This is in accord with the findings of the experiments at room temperature which predict negligible isomerization probability during ozone formation.[11]

V. CONCLUDING REMARKS

In this paper we argued that the threshold spectra of all isotopomers of ozone consist mainly of the van der Waals states in the two channels adjacent to the main well. States in each channel form vibrational progressions and preserve a large degree of independence from the states in the other channel and in the main ozone well. In conclusion, we would like to briefly discuss the limitations of the present study and to indicate the ways to refine the model we employed.

The spectrum discussed above is calculated for a nonrotating molecule, $J=0$. If ozone is formed in collisions of O atom with molecular oxygen, as in the atmosphere or in the lab measurements at room temperature,[11] the average value of the total angular momentum in the thermal ensemble is near $J=20$.[20] How does the overall rotation influence the properties of the vdW wells at threshold? In the asymptotic channel, the rotation of the molecule can be characterized with two quantum numbers, total angular momentum J and its projection on the body fixed a-axis, K_a. For a given K_a, the dissociation threshold lies $B_0K_a(K_a+1)$ above the lowest threshold ($B_0=1.4$ cm^{-1} is the rotational constant of a free $^{16}O_2$ diatom). Because of the large value of B_0 and a quadratic dependence of the threshold energy on K_a, only $K_a\approx 0$ states contribute significantly to the spectrum in the

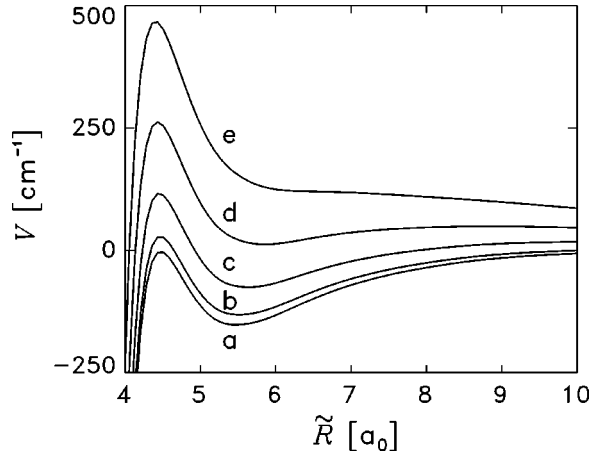

FIG. 9. The lowest adiabatic potential curves as functions of the Jacobi coordinate $\tilde{R}$ in the vdW region for five different total angular momenta: (a) $J=0$; (b) $J=10$; (c) $J=20$; (d) $J=30$; and (e) $J=40$. The projection K_a on the body fixed axis is zero.

vicinity of the first dissociation threshold.[20] The impact of J can be estimated using the adiabatic approximation discussed in the Introduction. Shown in Fig. 9 are the lowest adiabatic potential curves for several values of J and $K_a=0$ calculated using the Hamilton operator for a rotating molecule with the Coriolis interaction neglected (see Ref. 20 for details). All curves asymptotically converge to the threshold energy for $J=0$ because the centrifugal term $J(J+1)/R^2$ vanishes as $R\rightarrow\infty$. The centrifugal potential influences the vdW region in two ways. First, it increases the height of the adiabatic barrier to the main well; the vdW states in a rotating molecule are even less mixed with the ''normal'' states than those for $J=0$. More important, however, is that the rotation gradually destroys the vdW well itself; in the adiabatic approximation the local minimum disappears between $J=30$ and $J=40$. Thus, the Hamiltonian supports vdW states only in a limited range of J, and the number of such states in a given K_a block decreases with growing J. Adiabatic curves for small $K_a\neq 0$ are very similar to those depicted in Fig. 9. For large $K_a\sim J$ the vdW wells are again partly restored, but the price to be paid is a dramatic increase in the threshold energy which shifts the vdW wells far above the lowest dissociation threshold. Thus, the significance of the vdW states in a rotationally excited ozone diminishes, from the adiabatic viewpoint. Accurate quantum mechanical calculations testing this conclusion are currently under way.

While rotation apparently destroys the vdW spectrum, adjacent electronically excited states might support additional vdW states. Nine electronic states correlate with the lowest dissociation channel $O_2(X\,^3\Sigma_g^-)+O(^3P)$: three singlet, three triplet, and three quintet states. Potential energy curves for these states along MEP were recently calculated in Ref. 19. In addition to the ground electronic state, one singlet and two triplet states possess vdW minima capable of supporting vibrational states. The properties of the vdW states are further complicated by the strong spin–orbit coupling between the multiplets, which is dominated by the interaction in the $O(^3P)$ and which destroys spin as a good quantum number of ozone.[19] Spin–orbit interaction splits spin multiplets thus increasing the nominal number of electronic states with vdW minima from 4 to 8. The van der Waals dynamics should be investigated in all these states simultaneously, because the strength of the spin orbit coupling ($\sim 150\ cm^{-1}$) is of the order of the depth of the vdW well. Moreover, spin–orbit coupling shifts the lowest dissociation threshold 79.6 cm^{-1} downwards, placing it below the threshold of the adiabatic ground electronic state considered in this work.[19] This implies that some of the bound vdW states might turn into resonances if spin–orbit interaction is turned on. Disentangling the vdW dynamics in a network of coupled electronic states is one of the challenges in the future studies of ozone.

ACKNOWLEDGMENTS

Financial support by the Deutsche Forschungsgemeinschaft through the Sonderforschungsbereich 357 ''Molekulare Mechanismen Unimolekularer Reaktionen,'' the Fonds der Chemischen Industrie, and the Alexander von Humboldt-Stiftung is gratefully acknowledged.

[1] *Molecular Quantum States at Dissociation*, edited by R. Prosmiti, J. Tennyson, and D. C. Clary (CCP6, Daresbury, 1998).
[2] H. Ishikawa, R. W. Field, S. C. Farantos, M. Joyeux, J. Koput, C. Beck, and R. Schinke, Annu. Rev. Phys. Chem. **50**, 443 (1999).
[3] M. Joyeux, S. C. Farantos, and R. Schinke, J. Phys. Chem. A **106**, 5407 (2002).
[4] J. Weiss, J. Hauschildt, S. Yu. Grebenshchikov, R. Düren, R. Schinke, J. Koput, S. Stamatiadis, and S. C. Farantos, J. Chem. Phys. **112**, 77 (2000).
[5] D. A. Sadovski, N. G. Fulton, J. R. Henderson, J. Tennyson, and B. I. Zhilinski, J. Chem. Phys. **99**, 906 (1993).
[6] T. Azzam, R. Schinke, S. C. Farantos, M. Joyeux, and K. A. Peterson, J. Chem. Phys. **118**, 9643 (2003).
[7] A. Delon, F. Reiche, B. Abel, S. Yu. Grebenshchikov, and R. Schinke, J. Phys. Chem. A **104**, 10374 (2000).
[8] S. Heilliette, A. Delon, R. Jost, S. Yu. Grebenshchikov, R. Schinke, and J. C. Rayez, Z. Phys. Chem. (Munich) **215**, 1069 (2001).
[9] K. Mauersberger, Geophys. Res. Lett. **8**, 935 (1981).
[10] C. Janssen, J. Guenther, D. Krankowsky, and K. Mauersberger, J. Chem. Phys. **111**, 7179 (1999).
[11] C. Janssen, J. Guenther, K. Mauersberger, and D. Krankowsky, Phys. Chem. Chem. Phys. **3**, 4718 (2001).
[12] C. Janssen, J. Guenther, D. Krankowsky, and K. Mauersberger, Chem. Phys. Lett. **367**, 34 (2003).
[13] Y. Q. Gao and R. A. Marcus, Science **293**, 259 (2001).
[14] R. Siebert, P. Fleurat-Lessard, R. Schinke, M. Bittererovà, and S. C. Farantos, J. Chem. Phys. **116**, 9749 (2002).
[15] D. Babikov, B. K. Kendrick, R. B. Walker, R. T Pack, P. Fleurat-Lessard, and R. Schinke, J. Chem. Phys. **118**, 6298 (2003).
[16] D. Babikov, B. K. Kendrick, R. B. Walker, R. Schinke, and R. T Pack, Chem. Phys. Lett. **372**, 686 (2003).
[17] D. Babikov, B. K. Kendrick, R. B. Walker, R. T Pack, P. Fleurat-Lessard, and R. Schinke, J. Chem. Phys. **119**, 2577 (2003).
[18] S. Yu. Grebenshchikov, R. Schinke, and P. Fleurat-Lessard (unpublished).
[19] P. Rosmus, P. Palmieri, and R. Schinke, J. Chem. Phys. **117**, 4871 (2002).
[20] P. Fleurat-Lessard, S. Yu. Grebenshchikov, R. Siebert, R. Schinke, and N. Halberstadt, J. Chem. Phys. **118**, 610 (2003).
[21] M. Quack and J. Troe, Ber. Bunsenges. Phys. Chem. **78**, 240 (1974).
[22] D. J. Nesbit, Chem. Rev. **88**, 843 (1988).
[23] A. Rohrbacher, N. Halberstadt, and K. C. Janda, Annu. Rev. Phys. Chem. **51**, 405 (2000).
[24] L. Oudejans and R. E. Miller, Annu. Rev. Phys. Chem. **52**, 607 (2001).
[25] T. Xie, D. Wang, J. M. Bowman, and D. E. Manolopoulos, J. Chem. Phys. **116**, 7461 (2002).
[26] C. L. Russel and D. E. Manolopoulos, Chem. Phys. Lett. **256**, 465 (1996).
[27] D. Skouters, D. E. Manolopoulos, W. Bian, H.-J. Werner, L.-H. Lai, and K. Liu, Science **286**, 171 (1999).

[28] H. Hippler, R. Rahn, and J. Troe, J. Chem. Phys. **93**, 6560 (1990).
[29] T. H. Dunning, J. Chem. Phys. **90**, 1007 (1989).
[30] T. P. Grozdanov, V. A. Mandelshtam, and H. S. Taylor, J. Chem. Phys. **103**, 7990 (1995).
[31] M. R. Wall and D. Neuhauser, J. Chem. Phys. **102**, 8011 (1995).
[32] V. A. Mandelshtam and H. S. Taylor, J. Chem. Phys. **102**, 7390 (1995).
[33] T. A. Barker and G. I. Gellene, J. Chem. Phys. **117**, 7603 (2002).
[34] J. C. Light and T. Carrington, Adv. Chem. Phys. **114**, 263 (2000).
[35] J. Echave and D. C. Clary, Chem. Phys. Lett. **190**, 225 (1992).
[36] S. K. Gray and E. M. Goldfield, J. Phys. Chem. A **105**, 2634 (2001).
[37] M. J. Bramley and T. Carrington, Jr., J. Chem. Phys. **99**, 8519 (1993).
[38] Z. Bačić and J. C. Light, Annu. Rev. Phys. Chem. **40**, 469 (1989).
[39] S. Yu. Grebenshchikov, M. Joyeux, and R. Schinke (unpublished).
[40] R. T Pack and G. A. Parker, J. Chem. Phys. **87**, 3888 (1987).
[41] A. Chichery, A. Barbe, V. G. Tyuterev, and S. Tashkun, J. Mol. Spectrosc. **205**, 347 (2001).
[42] Since the nuclear spin of both ^{16}O and ^{18}O is zero, the nuclear spin statistical weights for the vibrational states with $P=-1$ identically vanish in a nonrotating molecule [see, for example, J. M. Hollas, *High Resolution Spectroscopy* (Wiley, New York, 1998)]. Strictly speaking, only symmetric ($P=+1$) states exist in C_{2v} ozone molecules prepared from these isotopes. In this paper we ignore the effects of nuclear spin and consider both parities on equal grounds.
[43] Spectra of ozone isotopomers at low energies were determined in a set of separate calculations which will be reported elsewhere.